Nonlinear model for thermal effects in free-electron lasers

E. Peter, A. Endler, and F. B. Rizzato

Citation: Physics of Plasmas (1994-present) **21**, 113104 (2014); doi: 10.1063/1.4901241
View online: http://dx.doi.org/10.1063/1.4901241
View Table of Contents: http://scitation.aip.org/content/aip/journal/pop/21/11?ver=pdfcov
Published by the AIP Publishing

Nonlinear model for thermal effects in free-electron lasers

E. Peter,[a] A. Endler,[b] and F. B. Rizzato[c]
Instituto de Física, Universidade Federal do Rio Grande do Sul, Caixa Postal 15051, 91501-970 Porto Alegre, RS, Brazil

(Received 3 September 2014; accepted 28 October 2014; published online 7 November 2014)

In the present work, we extend results of a previous paper [Peter *et al.*, Phys. Plasmas **20**, 12 3104 (2013)] and develop a semi-analytical model to account for thermal effects on the nonlinear dynamics of the electron beam in free-electron lasers. We relax the condition of a cold electron beam but still use the concept of compressibility, now associated with a warm beam model, to evaluate the time scale for saturation and the peak laser intensity in high-gain regimes. Although vanishing compressibilites and the associated divergent densities are absent in warm models, a series of discontinuities in the electron density precede the saturation process. We show that full wave-particle simulations agree well with the predictions of the model. © *2014 AIP Publishing LLC*. [http://dx.doi.org/10.1063/1.4901241]

I. INTRODUCTION

The presence of velocity spread in the transport of charged beams affects the overall system performance for any application where beams interact with ambient wave modes. Interestingly, not always is the spread detrimental. In the case of beams with inhomogeneous transverse profiles, for instance, a coplanar transverse velocity spread may actually prevent the appearance of strong nonlinear features like wave-breaking and the undesired associated emittance growth.[1] In most cases, however, fine tuning control between the beam velocity and the phase-velocities of the relevant wave modes present in the system is needed. Under these conditions, the usual requirement for a good quality beam is that the velocity spread of the beam be much smaller than all relevant velocity scales of the problem.

Free-electron lasers (FELs) fall in the latter class of system discussed in the preceding paragraph. Here, the electron beam interacts with the ponderomotive wave formed by the amplifying signal and a wiggler field, and a precise mismatch between the beam velocity and the phase-velocity of the ponderomotive wave is needed to optimise the interaction.[2,3] For an efficient interaction, in this case, one should avoid velocity spreads larger than the velocity difference between the beam and ponderomotive wave.[4,5]

The effects associated with velocity spreads in FELs have been studied over the years. In the present work, we investigate the issue by extending previous techniques based on the concept of compressibility. The compressibility has been proved useful to determine the transition from laminar to mixing regimes of cold, or monoenergetic, electron beams in FELs.[6] Compressibility, the inverse of the density function, vanishes at transition and indicates therefore the formation of singular fluid densities that foreshadow the onset of mixing in the phase-space of the electron beam.[7] As the electron beam undergoes mixing, coherence is lost and the amplifying signals saturates. Based on this set of features, a cold fluid model was then developed to estimate both the transition time and the saturated levels. The model was shown to agree well with wave-particle simulations.

We should like to perform a similar analysis, but now for a warm beam with a small but finite spread of longitudinal velocities. This poses an initial problem which comes from the fact that, in principle, even the laminar regime here requires a kinetic description based on the full phase-space. What we do to circumvent this difficulty, and still make use of the more familiar macroscopic fluid quantities like the compressibility, is to add a pressure term to the cold fluid model developed earlier. This technique has been applied in related beam systems[1] and revealed nice agreement with full simulations. We shall see that the agreement is remarkable in the present analysis as well, provided that the velocity spread be smaller than the velocity difference between beam and ponderomotive wave.

Our results show that the presence of infinite densities ceases to occur when the velocity spread is added, which is expected since spread is equivalent to the inclusion of temperature and the expanding effects of pressure in the fluid equations. However, preceding mixing regimes, one still encounters singularities, now arising from the formation of discontinuities in the compressibility and density. This is precisely what has been recently observed in the dynamics of inhomogeneous magnetically confined warm beams, where divergent density peaks of cold beams are replaced with density discontinuities as pressure is added to the system.[1] The basic program of the present work is then to compare wave-particle and fluid simulations based on the warm fluid model, as we investigate the role of velocity spreads in the instability, mixing, and saturation of FELs.

The paper is organized as follows: in Sec. II, we discuss the basic physical model; in Sec. III, we produce an analytical approximation for the resulting set of equations, investigate the problem, and compare the analytical approximation with results from full simulations; and in Sec. IV, we draw our conclusions.

[a]peterpeter@uol.com.br
[b]aendler@if.ufrgs.br
[c]rizzato@if.ufrgs.br

II. GOVERNING EQUATIONS

As already mentioned in the Introduction, the physical model has been developed in a previous paper.[6] We do not intend to cover all the steps again, but we need to see how the thermal effects come about in the simplified model. We shall start with a brief review of the governing equations for the full wave-particle dynamics and then proceed to the discussion of the appropriate warm fluid simplified model.

A. Full wave-particle equations

Let us first of all recall that particles move in the ponderomotive well formed by the laser ($\mathbf{A}$) and wiggler ($\mathbf{A}_w$) vector potential fields, respectively, given by

$$\frac{e\mathbf{A}}{mc^2} = a(z)\hat{\mathbf{e}}\exp i(k\,z - \omega\,t) + c.c.\,, \tag{1}$$

$$\frac{e\mathbf{A}_w}{mc^2} = a_w\hat{\mathbf{e}}\exp i(k_w\,z) + c.c.\,. \tag{2}$$

Variable $a = a(z)$ is the slowly varying dimensionless amplitude of the laser, and a_w is the dimensionless amplitude of the wiggler. The carrier's frequency and wavevector are, respectively, given by ω and k, and k_w is the wavevector of the wiggler; $\hat{\mathbf{e}}$ denotes the circular polarization versor, m and e are the electron mass and charge, and c is the speed of light. We note that the overall dynamics evolves along the propagation axis z on a steady-state regime.

Each of the N macroparticles in the ponderomotive well is governed by the pairs of equations

$$\frac{d\theta_j}{dz} = \left(\frac{v_{z_j}}{v_p} - 1\right), \tag{3}$$

$$\frac{d\gamma_j}{dz} = -\frac{a_w}{2\gamma_j}\left(ae^{i\theta_j} + c.c.\right) + v_{z_j}v_pE_z\left(\theta_j\right), \tag{4}$$

for $j = 1, 2, 3,\ldots N$. Variable $\theta_j \equiv k_pz_j - \omega t$ with $k_p \equiv k + k_w$ is the particle phase in the ponderomotive well, and γ_j is the relativistic factor given as

$$\gamma_j = \frac{\sqrt{1 + A_{tot}^2}}{\sqrt{1 - v_{z_j}^2}} \tag{5}$$

with $\mathbf{A}_{tot} = \mathbf{A}_w + \mathbf{A}$. We take $v_{z_j}/c \to v_{z_j}$ as the dimensionless electron velocity, and $v_p = \omega/ck_p \approx k/k_p$ as the dimensionless phase-velocity of the ponderomotive wave. In Eqs. (3) and (4), variable z denotes the dimensionless spatial coordinate co-moving with the ponderomotive wave: $k_pz = k_p(v_pt) \to z$.

The electric field $E_z(\theta)$ arises from space-charge effects and can be cast in the following appropriate form both for full simulations and for the upcoming fluid model:

$$E_z(\theta) = \pi\eta^2\left(\frac{N_- - N_+}{N}\right) + \eta^2\left(\langle\theta_j\rangle - \theta\right). \tag{6}$$

Here, $N_{-(+)}$ is the number of particles to the left (right) of coordinate θ ($N = N_- + N_+$), $\langle\theta_j\rangle$ is the center of mass of the distribution inside of the ponderomotive potential, and $\eta^2 = \omega_p^2/\omega^2$ is the space-charge factor arising from the beam charge; $\omega_p^2 = 4\pi n_0e^2/mc$ is the plasma frequency, with n_0 as the average density of particles.

Our final dynamical equation is the one governing the slowly varying amplitude of the stimulated radiation. It reads[2,8,9]

$$\frac{da}{dz} = \eta^2v_p\,a_w\left\langle\frac{e^{-i\theta_j}}{2\gamma_j}\right\rangle - i\eta^2v_p\left\langle\frac{1}{2\gamma_j}\right\rangle a, \tag{7}$$

with the brackets indicating an average over the electron distribution.

The set of nonlinear equations (1)–(7) describes the dynamics of a FEL with constant wiggler parameters a_w and k_w, taking into account the presence of space-charge effects. The set is generic in the sense that it provides the way to investigate, within its limits, arbitrary kinetic regimes. In the previous work, we focused on monoenergetic initial conditions. A simplified fluid model was then derived and analyzed. We intend to pursuit this kind of strategy, but now incorporating the effects of an initial spread of longitudinal velocities.

B. The warm fluid model

If the electron distribution has an initial spread of longitudinal velocities, even the corresponding initial laminar regime should be described by a kinetic approach. These regimes are nevertheless well approximated by warm fluid models,[10] provided that the velocity variance of an otherwise quite arbitrary distribution function remains small.[11] As a matter of fact, it has been shown that nonrelativistic water bag distributions with constant density over the occupied phase-space are exactly represented by adiabatic fluid equations,[12] as long as the laminar regimes persists.

Given the simplicity and the reach of water bag distributions, at this point, we introduce our initial distribution function for electrons as a uniform water bag lying along the phase θ, with a small half-width Δv_0 around an average injection velocity v_0. We point out that due to the smallness of the velocity width, a very realistic assumption for FELs,[13] the connections between the widths in velocity, momentum, and energy spaces are approximately linear. Under the linearity condition, if the phase-space density is a constant in one representation, it is also constant in the others. With views at the warm fluid modeling, this is why we decided to work with the velocity space.

As we build the warm fluid model from the fully kinetic initial condition introduced in the preceding paragraph, we observe that not only is the width Δv_0 small, but also are velocity excursions away from their initial values.[6] We can therefore switch from the original variables θ and γ to the more recognizable phase-space pair θ, $\dot{\theta}$, with the needed relation between general small deviations for $\dot{\theta}$ and γ from their respective averages given in the form $\delta\gamma = 2k_p^{-1}\gamma D_\gamma\delta\dot{\theta}$ ($\delta\dot{\theta} = d\delta\theta/dz$), where $D_\gamma \equiv \partial v/\partial\gamma^2$.

Within this linear approximation, one recovers all terms of the fluid equation, Eq. (10) of Ref. 6, with the remarkable

addition of a term accounting for the velocity spread effects—details are discussed in the Appendix. The full equation for the phase is written in the form

$$\frac{\partial^2\theta}{\partial z^2} = -\frac{D_\gamma}{v_p}\left[a_w\tilde{a}(z)e^{i\theta} + c.c.\right] + 2v_p\eta^2 D_\gamma\gamma_r(\theta_0-\theta) + (\Delta v_0)^2\frac{\partial^2\theta}{\partial\theta_0^2}\left(\frac{\partial\theta}{\partial\theta_0}\right)^{-4}, \quad (8)$$

with $\tilde{a}(z) = a(z)e^{-i\nu z}$ and ν as the small frequency detuning associated with the dimensionless velocity mismatch $\nu \equiv (v_0 - v_p)/v_p$. The term proportional to η^2 is the approximation for the space-charge term, developed in the same mentioned reference under the condition that fluid elements do not overtake each other.[6] We note that the convenient inclusion of the detuning ν into a rescaled laser field allows to take the initial value of fluid variable $\dot{\theta}$ in the simplified model as zero.

Equation (8) is the approximate governing equation for the phase θ as obtained and discussed in the Appendix. In contrast to its form when the spread is neglected, Eq. (8) is to be viewed as a nonlinear partial differential equation for θ in Lagrangian coordinates θ_0 and z, the nonlinear differential coupling generated by the velocity spread. We recall that according to the Lagrangian representation, the phase θ plays the role of a field variable evolving along the *time* z from an initial condition θ_0: $\theta = \theta(\theta_0, z)$.[14]

With basis on Eq. (8), the corpuscular electron population has been converted into an averaged charged fluid that can be analyzed with similar tools as those used in Ref. 6. In particular, we shall look for singularities in the compressibility, as those indicate the onset of mixing leading to saturation. The compressibility is defined in the form $C \equiv \partial\theta/\partial\theta_0$ and allows to express the fluid density in the laminar regime as $n = n_0/C$, with n_0 as the unperturbed density. Zeros and singularities in C are tantamount to singularities in n, which typically announce the breakdown of laminar fluid regimes.

On a final and essential note before proceeding to the numerical analysis of the system, we observe that Eq. (8) needs $a = a(z)$ as an input. In that regard, it had been observed in Ref. 6 that while details of the particle dynamics leading to saturation must be described with the cold version of nonlinear equation (8), the exact radiation field closely follows its linear version up to the onset of mixing.

To calculate $a(z)$, we therefore stick to the linear approach, which for all practical purposes we base on the effective warm fluid model developed here. To do that, one first observes that as the pressure term of Eq. (8) is linearized and the second derivative $\partial^2\theta/\partial\theta_0^2$ is approximated by the dominant harmonic $-(\theta-\theta_0)/(2\pi)^2$, the resulting effect of the thermal spread on the longitudinal dynamics is to "renormalize" the space-charge factor in the electronic momentum equations, already present in cold beams. As for the transverse electron dynamics, needed to evaluate the source terms in Eq. (7), we shall approximate γ as its local velocity average over the electron distribution.

We are therefore making the assumption that the longitudinal pressure term is the one ruling the kinetic effects, which will be shown shortly to be a reasonably accurate assumption under the conditions of the present analysis.

Following all these approximative maneuvers, we obtain the stimulated laser field from a set identical in form to the linear set obtained in Ref. 6, with the solely difference being that the space-charge factor of the cold version is replaced according to the rule $\eta^2 \to \eta^{*2} \equiv \eta^2 + \Delta v_0^2/4\pi^2 D_\gamma\gamma_r v_p$ in the momentum equation. The "renormalized" linear set takes the form

$$\frac{d\tilde{a}}{dz} = -i\frac{v_p\eta^2}{2\gamma_r}a_w X - \frac{v_p\eta^2}{2\gamma_r^2}a_w Y - i\frac{v_p\eta^2}{2\gamma_r}\tilde{a} + i\nu\tilde{a}, \quad (9)$$

$$\frac{dX}{dz} = \frac{2}{v_p}D_\gamma\gamma_r Y - i\frac{a_w}{v_p}D_A\tilde{a}, \quad (10)$$

$$\frac{dY}{dz} = -v_p^2\eta^{*2}X - \frac{1}{2\gamma_r}a_w\tilde{a}, \quad (11)$$

where $X \equiv \langle\delta\theta e^{-i\theta_0}\rangle = (2\pi)^{-1}\int_0^{2\pi}\delta\theta e^{-i\theta_0}d\theta_0$ and $Y \equiv \langle\delta\gamma e^{-i\theta_0}\rangle = (2\pi)^{-1}\int_0^{2\pi}\delta\gamma e^{-i\theta_0}d\theta_0$ are the bunching factors for the warm fluid version of the electron beam.

The linear set is then solved to produce a linearly growing field $a(z)$ whose growth rate is maximized by a convenient choice of the detuning ν, a critical parameter for optimization.

In Fig. 1, we briefly depict a comparison of the maximizing detuning as a function of the spread Δv_0, both from the full simulations and from the simplified warm fluid model. It is seen that despite the approximation based on the smallness of the velocity spread used for the warm fluid model, both results agree well. As a matter of fact, slight deviations can be observed from $\Delta v_0 = 0.001$ on, but those do not affect the general adequacy of the model within the range we are interested in. In this paper, we restrict our range up to the limit $(\Delta v_0)_{max} \sim \nu \sim 0.002$, where the spread becomes comparable to the maximizing velocity mismatch, as suggested by Fig. 1, and the interaction efficiency diminishes. We observe that under condition $\nu > \Delta v_0$, we can also see our system as in a hydrodynamical regime.[15] The hydrodynamical regime therefore survives until $\Delta v_0 \sim \nu$, beyond which it becomes kinetic. The transition is not sharply defined, but with help of the linear dispersion relation one can solve for the corresponding Δv_0 satisfying the previous

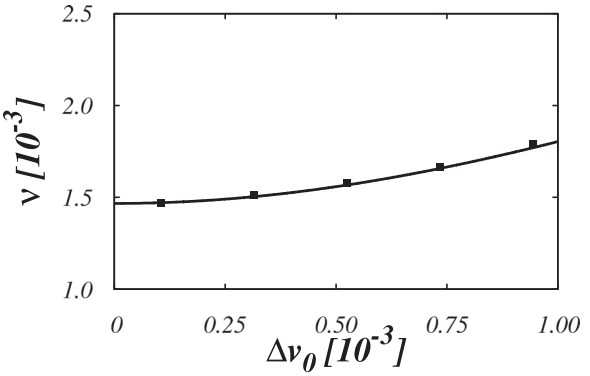

FIG. 1. The detuning ν for the maximum growth rate versus the spread Δv_0. Solid line obtained from the semi-analytical model and filled squares from simulations.

similarity condition. In an approximative way, calculating the maximizing ν in terms of η with help of the cold beam dispersion relation, we can estimate the transition value for Δv_0 directly in terms of the space-charge factor. The expression is extensive, but if one consults its graphical representation offered by Fig. 2 in Ref. 6, one sees that the transition can be identified by the characteristic spread $\Delta v_0 \sim 0.0015$, which agrees with the magnitudes discussed above. As one reduces the spread, the beam gradually tends to the cold limit.

Finally, the growth rate is obtained from simulations through a linear fitting for the numerically obtained $\log(|a(z)|)$. In terms of magnitude, it falls close—within a range of 6%—from calculations involving different kinds of distribution function.[13]

Considering the importance of space-charge effects in many current devices,[16] in all cases investigated in this paper, we take $\eta = 0.03$, unless otherwise stated, which places the system in a high-gain Raman regime,[2,17,18] $v_p = 0.99$ and $a(z=0) = -ia_w \times 10^{-5}$ with $a_w = 0.4$. The number of macroparticles used in the simulations ranged from $N = 2000$ to $N = 10\,000$.

III. NONLINEAR FEATURES FROM SIMULATIONS AND MODEL

A. Laminar versus mixing regimes

As a first step in our analysis, we shall determine basic features of the transition from laminar to mixing regimes of our system.

When thermal effects are neglected, the transition can be identified with help of singularities in the electron density.[6] At the transition, the compressibility vanishes and the density diverges, which reflects the fact that the laminar electron distribution of cold beams is twisted in a way that one can no longer establish single fluid variables at the same θ. For sufficiently large values of the space-charge factor η, this kind of behaviour has been recognized in previous investigations as similar to wave-breaking processes.[6,19–21]

Let us now see what happens when $\Delta v_0 \neq 0$.

Figure 2 compares results from simulations and from the model. In panels (a) and (b), we depict the density, as obtained from compressibility calculations based on the model equation, Eq. (8), respectively, for $\Delta v_0 = 0.0002$ and $\Delta v_0 = 0.001$. In panels (c) and (d), we plot the respective phase-spaces.

The key ingredient to fabricate the figures is that the density plots capture instants where the compressibility and density are just about to become discontinuous. We denote these special instants as z_b, with b standing for *breakdown*. The meaning of this discontinuity is that fronts with different densities collide at the same phase coordinate. This view is confirmed as we examine the snapshots of the fully simulated phase-space dynamics in panels (c) and (d). The snapshots, revealing fingers that protrude from the lower border of the electron distribution, are also taken at the precise instant—nearly the same as in the density counterparts—where the density (obtained as an integral along the vertical axis) at both sides of the left boundary of the fingers becomes discontinuous as well.

Some features are then worthy of note. (i) We first emphasize the nice agreement between the warm fluid model and full simulations, both of which producing the discontinuities nearly at the same instant. (ii) As we examine the phase plots, we conclude that discontinuities are in fact a prelude to the process of mixing where the contours of the electron distribution can no longer be described as a single valued structure. From that moment on, the growing stimulated radiation field tends to saturate. This is seen in Fig. 3, where the laser amplitude, obtained for $\Delta v_0 = 0.0002$, starts to deviate from the linear growth nearly at the time predicted in panels (a) and (c) of Fig. 2. (iii) Smaller spreads are associated with

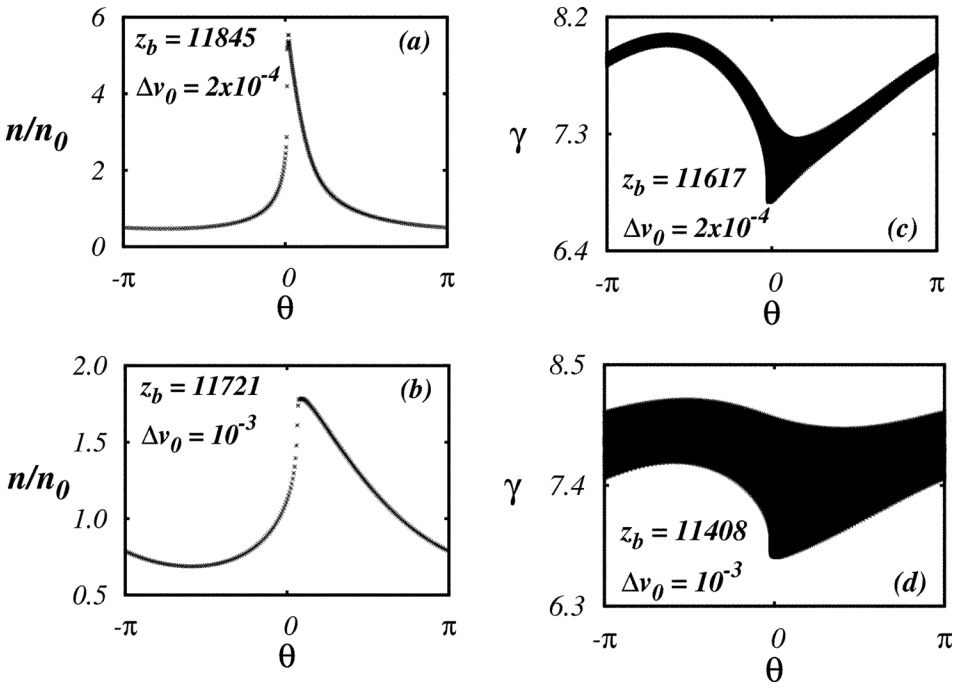

FIG. 2. Comparison of density plots (a) and (b) and respective phase-spaces (c) and (d).

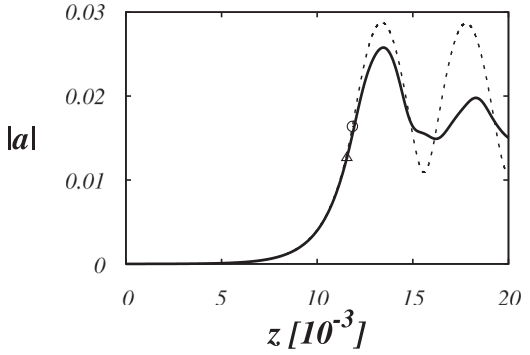

FIG. 3. Amplitude of the stimulated radiation against time: full simulations represented by the solid line, approximate model based on estimated values for the bunching factors represented by the dotted line. Circle (triangle) indicates the breakdown time according to the model (full simulations); $\Delta v_0 = 0.0002$.

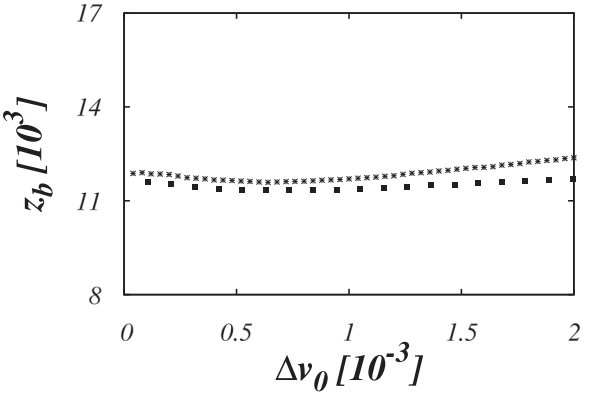

FIG. 4. Plots of z_b versus the spread Δv_0, both from full simulations (filled squares) and model (stars).

larger discontinuities; in particular, cold electrons beams produce infinite discontinuities associated with the divergent densities observed in Ref. 6. (iv) It is known that not all the electrons of warm beams are active participants in the FEL interaction. The compressibility may be a useful tool to investigate the issue since, from what we see here, the active fraction directly relates to the size of the discontinuities of the density, the inverse of the compressibility. Indeed, while large discontinuities are associated with a large active fraction, small discontinuities associate with small fractions in the protruding fingers. Although we still lack a more precise quantitative analysis here, we note that in the case of panels (a) and (c), where densities disturbances are large, all particles at the density peak are captured in the rotating finger. On the other hand, in the case of panels (b) and (d), where disturbances are small, an equivalently small fraction of electrons forms the finger.

All in all, we conclude that saturation in systems with thermal spread is signaled by the presence of discontinuities in the compressibility factor, or, alternatively, in the density of the electronic fluid. These discontinuities are seen to appear as the laminar regimes breakdown and give place to mixing and saturation.

B. Time span for the laminar regime

As seen in Subsection III A, the laminar regime extends up to the point where the fluid description based on single valued contours breaks down. From that point on, mixing sets in and the stimulated mode ceases to grow. The breakdown time z_b is a critical time scale for our problem and in both simulations and model we search for it as the first instants where for some value of θ either the compressibility of the warm fluid model or the density in the full simulations develop discontinuites.

The result of the comparison is displayed in Fig. 4 and shows reasonable agreement between model and simulations as already suggested by the discussion of the subsection III A. We see that the breakdown time does not actually depend too heavily on the spread Δv_0, exactly as it had been revealed in Ref. 1. In fact, since we are investigating a hydrodynamic regime where the gap between the ponderomotive wave velocity and the beam velocity is larger than the velocity spread, the dynamics en route to the breakdown point depends weakly on Δv_0. The crucial feature here is the way the breakdown takes place, as commented earlier. When the breakdown point is reached, the small compressibility of Eq. (8) generates a large contribution of the thermal term and a resulting change on the density profile as compared with the cold beam case. In general we see that the breakdown time z_b is associated with density discontinuities of warm beams, the discontinuities evolving into divergences as Δv_0 goes to zero.

C. Saturation peak of the stimulated radiation

Once one has the breakdown time, which marks the onset of the saturation process for the FEL interaction, one can estimate the intensity of the first peak of radiation. The approach employed here is based on what has been observed in Ref. 6. In that cited paper, as already discussed earlier, it has been seen that the stimulated field grows much like its linear approximation, the deviation first appearing close to the first peak where the exact field saturates.

Given this relative accuracy of the linear approximation up to breakdown, we adopt the following strategy: we let the full linear system evolve up to z_b and freeze the bunching factors X and Y at that time, in an attempt to emulate the saturated state. From this point on, we accompany the newly acquired oscillatory motion of the laser amplitude and capture its first maximum.

The comparison of simulation and model can be found in Table I. A graphical representation for the model can also be seen as the dashed curve of Fig. 3 where we indicate the

TABLE I. Comparison of full simulations and analytical estimates for the first peak of the laser amplitude.

Δv_0	a^{peak}_{simul}	a^{peak}_{model}
0.0002	0.026	0.028
0.0006	0.023	0.019
0.0011	0.019	0.014
0.0015	0.015	0.012
0.0020	0.012	0.009

modeled (circle) and fully simulated (triangle) breakdown times.

The hypotheses of linearity and of a strictly constant bunching in the mixing phase introduce additional approximations to the model, but in spite of these the table still reveals a reasonable agreement between simulations and model.

Considering the simplicity of the steps adopted here to estimate the peak, we believe that the table serves its purposes.

D. Role of space-charge

Up to the present point, we have been using a fixed, and large, value for the space-charge factor η in our analysis: $\eta = 0.03$. We would like to conclude our analysis with a brief but more extended view on the role of space-charge in the system dynamics. The discussion is based on panels (a) and (b) of Fig. 5. Panel (a) represents the size of the density discontinuity as a function of η, and panel (b) represents the breakdown time z_b also as a function of η. Both figures are generated with the semi-analytical model, which was already seen to agree very well with full simulations. To evaluate the density discontinuities in a quick and reliable way, we uniformly partition the horizontal (θ) axis of the density plots into a large number of discrete elements and select the one with the largest density variation at the breakdown time. Partitions with 100 to 150 elements produce similar results. Again, this agrees with the jump in density obtained when we perform integrations of the phase-space density along the vertical axis. Note that the jump appears as we move across the left vertical boundaries of the protruding fingers of the phase-space plots, as for instance seen in Figs. 2(c) and 2(d).

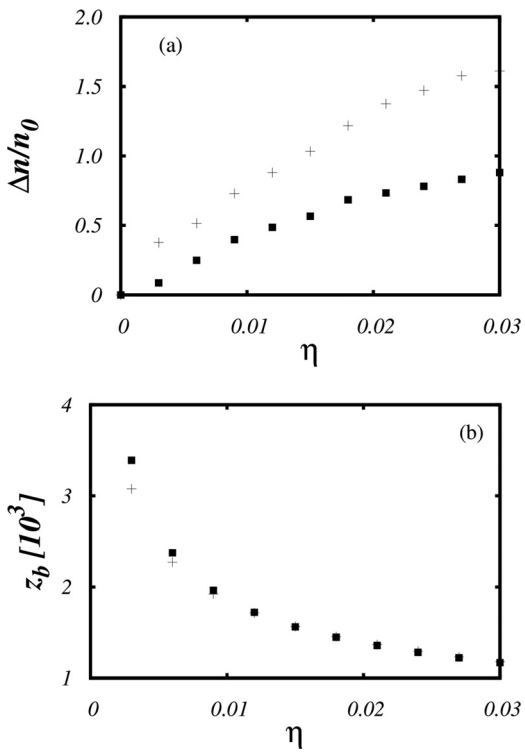

FIG. 5. Effect of space-charge on the density discontinuities (a) and on the breakdown time (b). Crosses represent $\Delta v_0 = 0.0002$ and filled squares $\Delta v_0 = 0.0004$.

From Fig. 5, we first notice that divergences are suppressed in thermal cases, as already commented along the text. We also observe that discontinuities tend to increase with η, the expected behavior when thermal effects become relatively small, with the beam looking gradually more like a cold one. Also, smaller spreads are associated with larger discontinuities.

Panel (b) reveals richer behavior. First of all, smaller values of η are associated with slower dynamics and larger breakdown times, the expected result arising from shallower ponderomotive wells. At larger value of η, region of hydrodynamical regimes, z_b, is quite insensitive to the spread. This is what we commented earlier when we discussed the relative constancy of z_b against the spread, seen in Fig. 4. However, when we abandon the hydrodynamical regimes at small η's, the spread can no longer be considered a small term, acquiring a noticeable effect on the breakdown time. Panel (b) complements the information gained earlier in the text, when we focused attention on the hydrodynamical regimes.

IV. CONCLUSIONS

In the present paper, we developed a nonlinear model to investigate the effects of longitudinal thermal spreads on the dynamics and relaxation of free-electron lasers. The analysis was based on the concept of the compressibility, a quantity directly associated with the electron density in the laminar regime. Compressibility was discussed in a previous paper where cold beams were examined and duly adapted here to deal with warm beams.

Spatial discontinuities of the compressibility were shown to signal the transition from laminar to mixing regimes. This feature was examined with an approximate set of nonlinear fluid equations, in a similar fashion to what has been recently done in the case of magnetically confined warm beams. Once again we observed that the transition in warm beams is preceded by discontinuities in the electron densities, rather than the density divergences seen in cold cases. The discontinuities were shown to be associated with the singular behavior of the lower boundary of the electronic distribution.

We made use of an initial water bag distribution for the electron population, which sets the system in an adiabatic regime during the laminar phase. Comparison between water bag and Maxwellian distributions has been made in similar systems showing good agreement between both.[11] Also, the magnitude of growth rates calculated here are comparable to those obtained for instabilities of Maxwellian distributions in the same physical setting. The agreement observed in those two instances suggests that the adiabatic approach is of relevance in the present matter.

We detect the breakdown time in simulations as the instant where the lower border of the distribution starts to twist around itself. This particular criterium, appropriate to sharply defined electron distributions, can be adapted to more general cases. One possibility is to pinpoint the onset

of mixing through the abrupt growth of the beam emittance, which has already been done in related systems.[1]

One also observes that our approximation on the connection between momentum and velocity is limited by the magnitude of the initial velocity spread Δv_0. However, given the narrow spreads in FELs,[13] the linear connection is fairly accurate.

As we mention along the work, the present strategy based on the compressibility suggests a way to estimate the fraction of the electron population actively participating in the FEL interaction. Figure 2 indeed showed that large and small discontinuities are, respectively, related to large and small fractions of participants: the larger the discontinuity, the larger the number of particles in the protruding finger. This issue and others, like the effects involved with the diffraction of the stimulated signal, are of relevance for the optimisation and efficiency of the FEL interaction. They shall be further studied in coming works as the appropriate quantitative analysis is developed.

ACKNOWLEDGMENTS

This work was supported by CNPq and FAPERGS, Brazil, and by the Air Force Office of Scientific Research (AFOSR), USA, under the Grant FA9550-12-1-0438. The authors wish to thank useful discussions with Renato Pakter and Antônio Serbeto.

APPENDIX: DERIVATION OF THE NONLINEAR WARM FLUID MODEL

Considering the phase-space θ, $\dot{\theta}$, the electronic density $n = n(\theta, z)$ can be expressed in terms of the electronic distribution function $f = f(\theta, \dot{\theta}, z)$ in the form

$$n(\theta, t) = \int f(\theta, \dot{\theta}, z) d\dot{\theta}. \tag{A1}$$

Neglecting the effects of collisions, the electronic distribution function must satisfy the Vlasov equation

$$\frac{\partial f}{\partial z} + \dot{\theta}\frac{\partial f}{\partial \theta} + \ddot{\theta}\frac{\partial f}{\partial \dot{\theta}} = 0. \tag{A2}$$

Taking the first-order moment of the Vlasov equation ($\int f \dot{\theta} d\dot{\theta}$) for a water bag distribution of half-width $\Delta\theta_0$, we obtain

$$\left(\frac{\partial \bar{\dot{\theta}}}{\partial z} + \bar{\dot{\theta}}\frac{\partial \bar{\dot{\theta}}}{\partial \theta}\right) + \frac{1}{mn}\left(\frac{\partial p}{\partial \theta}\right) - \ddot{\theta} = 0, \tag{A3}$$

where the pressure p for a unidimensional problem is written as[12]

$$p = m\left(\frac{\Delta\dot{\theta}^2}{3n_0^2}\right)n^3. \tag{A4}$$

In Eq. (A3), we can identify the thermal contribution to the system dynamics as

$$\left(\frac{\partial^2\theta}{\partial z^2}\right)_{ther} = -\frac{1}{mn}\left(\frac{\partial p}{\partial \theta}\right), \tag{A5}$$

which according to the equalities involving the compressibility $C \equiv \partial\theta/\partial\theta_0 = n_0/n$, takes the form

$$\left(\frac{\partial^2\theta}{\partial z^2}\right)_{ther} = -\Delta v_0^2\left[\frac{\partial\delta\theta}{\partial\theta_0} + 1\right]^{-4}\frac{\partial^2\delta\theta}{\partial\theta_0^2}, \tag{A6}$$

if we define $\delta\theta \equiv \theta - \theta_0$ and apply our normalization scheme.

The fluid equation, with term (A6) added, is the one introduced by Eq. (8) and used in the paper.

[1]E. G. Souza, A. Endler, F. B. Rizzato, and R. Pakter, Phys. Rev. Lett. **109**, 075003 (2012).
[2]R. Bonifacio, F. Casagrande, G. Cerchoni, L. de Salvo Souza, P. Pierini, and N. Piovella, Riv. del Nuovo Cimento **13**, 1 (1990).
[3]H. P. Freund and T. M. Antonsen, *Principles of Free-Electron Lasers* (Chapman and Hall, London, 1996).
[4]T. C. Marshall, *Free-Electron Lasers* (Macmillan Publishing Company, New York, 1985).
[5]C. Brau, *Free-Electron Lasers* (Academic Press, London, 1990).
[6]E. Peter, A. Endler, F. B. Rizzato, and A. Serbeto, Phys. Plasmas **20**, 123104 (2013).
[7]O. A. Anderson, Part. Accel. **21**, 197 (1987).
[8]F. B. Rizzato, Phys. Rev. A **14**, 1629 (1990); G. I. de Oliveira, F. B. Rizzato, and A. C. Chian, Phys. Rev. E **52**, 2025 (1995).
[9]J. T. Mendonça, *Theory of Photon Acceleration* (IOP Publishing, Bristol, 2001).
[10]R. C. Davidson and H. Qin, *Physics of Intense Charged Particle Beams in High Energy Accelerators* (World Scientific, Singapore, 2001).
[11]C. Chen, F. B. Rizzato, and R. Pakter, in *Proceedings of IPAC*, edited by C. Petit-Jean-Genaz (CERN, San Sebastián, Spain, 2011), p. 694.
[12]T. P. Coffey, Phys. Fluids **14**, 1402 (1971).
[13]A. Chakhmachi and B. Maraghechi, Phys. Plasmas **16**, 043110 (2009).
[14]R. M. G. M. Trines, Phys. Rev. E **79**, 056406 (2009).
[15]K. V. Lotov and I. V. Timofeev, "Transition regime of the one-dimensional two-stream instability," e-print arXiv:1408.2349v1 (2014).
[16]G. Marcus, E. Hemsing, and J. Rosenzweig, Phys. Rev. Spec. Top. Accel. Beams **14**, 080702 (2011).
[17]P. Sprangle, C.-M. Tange, and W. M. Manheimer, Phys. Rev. A **21**, 302 (1979).
[18]L. F. Monteiro, A. Serbeto, K. H. Tsui, J. T. Mendonça, and R. M. O. Galvão, Phys. Plasmas **20**, 073101 (2013).
[19]J. M. Dawson, Phys. Rev. **113**, 383 (1959).
[20]F. B. Rizzato, R. Pakter, and Y. Levin, Phys. Plasmas **14**, 110701 (2007).
[21]E. G. Souza, A. Endler, R. Pakter, F. B. Rizzato, and R. P. Nunes, Appl. Phys. Lett. **96**, 141503 (2010).